

## Dynamic Modeling and Analysis of Arch Bridges Using Beam-Arch Segment Assembly

Wei-Xin Ren<sup>1,2,3</sup>, Cong-Cong Su<sup>1</sup> and Wang-Ji Yan<sup>1</sup>

**Abstract:** A beam-arch segment assembly procedure is presented in this paper for the dynamic modelling and analysis of arch bridges. Such a beam-arch segment assembly is composed of different structural elements of arch bridges such as arch ribs (curved beams), suspenders, girders and floor beams. Based on the energy principle in structural dynamics, the stiffness matrix and mass matrix of such an assembly are formulated. The proposed procedure is then implemented to carry out the free vibration analysis of the Jian concrete filled tubular arch bridge. It is demonstrated that the proposed beam-arch segment assembly procedure is efficient with the advantages of less element numbers and enough accuracy. It is expected that this methodology can be an effective approach for the further dynamic response analysis of arch bridges under all kinds of dynamic loads such as earthquakes, winds and vehicles.

**Keywords:** finite element method; assembly; arch bridge; natural frequency; mode shape; ambient vibration test

### 1 Introduction

The arch bridge is often regarded as an aesthetic form of bridge. Its history can be traced to circa 3600 B.C. in the ancient kingdoms of Egypt and Mesopotamia [Peng and Fairfield (1999)]. China's oldest surviving stone masonry arch bridge, Zhao Zhou Bridge, dated back to 500 A.D., has withstood earthquakes, floods, traffic loading and weathering and still bears witness to it [Qian (1987)]. Various aspects of the history and development of the arch bridge were discussed [Billington (1977); Burden (1993)]. Compared with other types of bridge superstructures, arch bridges transmit the applied loads to the supports primarily through axial compression in the arch ribs while bending moments are relatively small. Moreover, with

---

<sup>1</sup> Department of Civil Engineering, Central South University, Changsha, 410075, China

<sup>2</sup> National Engineering Laboratory for High Speed Railway Construction, Changsha, 410075, China

<sup>3</sup> Corresponding author. Tel: +86-731-82654349; Fax: +86-731-85571736. E-mail: renwx@mail.csu.edu.cn (W.-X. Ren)

some other merits such as high strength, good seismic behavior and convenience of construction, arch bridges are still one of the main bridge types in the field of bridge engineering in recent decades [Nazmy (1997)].

Dynamic analysis of arch bridges has been carried out through theoretical, numerical and experimental analysis by many researchers [Raithel and Franciosi (1984); Lee and Wilson (1989); Roeder, Macrae, Crocker, Arima and Wong (2000); Nonaka and Ali (2001); Calcada, Cunha, Delgado (2002); Ren and Zong (2004); Zong, Jashi, Ge and Ren (2005)]. Theoretical methods involved in solving differential equations can provide exact solutions. However, the limitations are such that the behavior of complex surroundings and creations of arch bridges can not be completely described in one operation. During past five decades, the finite element method has rapidly become a very popular technique for the numerical solution of complex arch bridges. The finite element method is the most general and versatile method for analysis of structural problems. The conventional finite element method, however, may be too general to conveniently represent structural behavior in global for a specific type of bridge due to so many elements and output information involved. For some circumstances such as the vehicle-bridge interaction vibration analysis of complex bridges, it is still an issue to reduce the element number or degree of freedoms even with today's computational capacity.

Thus the process of subdividing the structure into the individual components, whose behavior is readily understood, and then rebuilding the original structure from such components has been another natural and effective way. With this regard, a assembly procedure named "beam-arch segment assembly" is proposed in this paper for the dynamic analysis of arch bridges. Such a segment assembly is composed of different supper-structural elements of arch bridges such as a curved-beam element for arch ribs, a truss element for suspenders and beam elements for floor beams and girders. The beam-arch segment assembly is able to treat the bridge segment composed of several different materials and different kinds of elements as a unit whole element naturally. Therefore, the advantage of the proposed approach, in contrast with the conventional finite element method, is that the beam-arch segment assembly reduces the number of degrees of freedom dramatically and simplifies the calculation.

In the proposed procedure of beam-arch segment assembly for the dynamic analysis of arch bridges the segment between two adjacent suspenders is regarded as one assembly. The super-structure of an arch bridge is firstly discetized into a number of segments. For each segment, the reasonable spatial displacement modes incorporated with the arch ribs, suspenders, and bridge deck are conceived. Then the total potential energy of elastic force and inertia force for the beam-arch segment assembly can be computed respectively. Based on the minimum principle of to-

tal potential energies in elastic system and corresponding forming matrix method [Zeng and Guo (1999); Zeng (2000)], the stiffness matrix and mass matrix of such a beam–arch segment assembly can be derived. Afterwards, the global stiffness matrix and mass matrix of an arch bridge can be obtained through assembling the matrixes of each beam–arch segment assembly. To demonstrate the applicability and efficiency of presented approach, the beam–arch segment assembly procedure is used to carry out the free vibration analysis of the Jian concrete-filled steel tube (CFST) arch bridge in Jangxi Province, China that was tested under operational vibration conditions. The obtained natural frequencies and mode shapes of the bridge are compared with those obtained from the commercial finite element software ANSYS (1994) and field ambient vibration testing. It is demonstrated that the proposed beam–arch segment assembly procedure for the dynamic analysis of arch bridges has less element numbers and achieves enough accuracy. It is expected that proposed beam–arch segment assembly procedure can be effectively used for the further complex dynamic response analysis of arch bridges under all kinds of dynamic loads such as earthquakes, winds and vehicles.

### 1.1 Formulation of beam-arch segment assembly

#### 1.2 Beam-arch segment

The super-structure of an arch bridge is normally composed of suspenders (columns), bridge deck and arch ribs. The segment between two adjacent suspenders can be regarded as one assembly named as “beam-arch segment assembly” as shown in Fig. 1. It can be seen that such a compound segment is made of different structural elements of arch bridges such as suspenders, girders (or tie bars), floor beams and arch ribs (curved beams).

Take a single (the  $e$ th) segment, as shown in Fig. 2, as an example. In the global coordinate system  $x$ - $y$ - $z$ , the segment assembly nodal displacement vector is defined by:

$$\{\delta_i\} = \begin{bmatrix} u_{ULi} & v_{ULi} & w_{ULi} & \theta_{xULi} & \theta_{yULi} & \theta_{zULi} & u_{URi} & v_{URi} & w_{URi} \\ \theta_{xURi} & \theta_{yURi} & \theta_{zURi} & u_{LLi} & v_{LLi} & w_{LLi} & \theta_{xLLi} & \theta_{yLLi} & \theta_{zLLi} \\ u_{LRi} & v_{LRi} & w_{LRi} & \theta_{xLRi} & \theta_{yLRi} & \theta_{zLRi} \end{bmatrix}^T \quad (1a)$$

$$\{\delta_j\} = \begin{bmatrix} u_{ULj} & v_{ULj} & w_{ULj} & \theta_{xULj} & \theta_{yULj} & \theta_{zULj} & u_{URj} & v_{URj} & w_{URj} \\ \theta_{xURj} & \theta_{yURj} & \theta_{zURj} & u_{LLj} & v_{LLj} & w_{LLj} & \theta_{xLLj} & \theta_{yLLj} & \theta_{zLLj} \\ u_{LRj} & v_{LRj} & w_{LRj} & \theta_{xLRj} & \theta_{yLRj} & \theta_{zLRj} \end{bmatrix}^T \quad (1b)$$

where  $\delta_i$  and  $\delta_j$  are the displacement vectors on the  $i$ th and  $j$ th sides of the segment assembly.  $u, v$  and  $w$  denote the displacements along  $x$ -axes,  $y$ -axes and  $z$ -axes,

respectively;  $\theta_x$ ,  $\theta_y$  and  $\theta_z$  denote the rotations about  $x$ -axes,  $y$ -axes and  $z$ -axes, respectively.  $UL_i$ ,  $LL_i$ ,  $UR_i$ ,  $LR_i$ ,  $UL_j$ ,  $LL_j$ ,  $UR_j$  and  $LR_j$  are the eight nodes of such a segment assembly where the first letters  $U$  and  $L$  denote the segment assembly's upper and lower nodes, while the second letters  $L$  and  $R$  denote the segment assembly's left (front) and right (back) nodes.

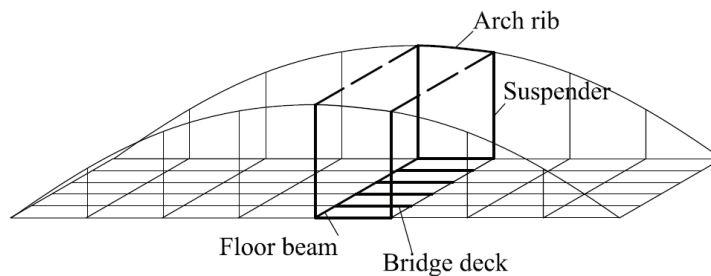


Figure 1: Sketch of a beam-arch segment assembly

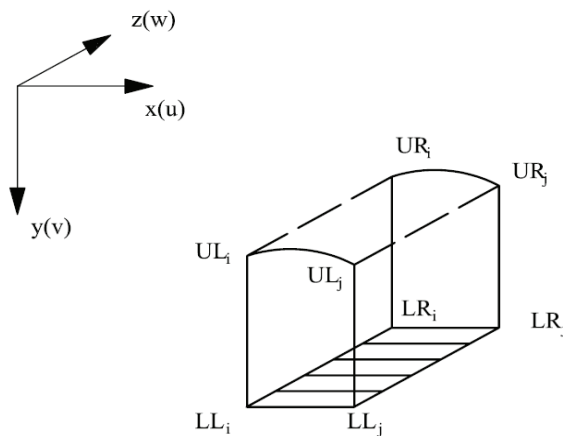


Figure 2: The  $e$ th beam-arch segment assembly

### 1.3 Curved beam element for arch ribs

It has been usually proposed to approximately model the arch rib by straight beam elements, which will degrade numerical efficiency. Considering that the arch rib

plays an important role in the load transferring of arch bridges, the number of the straight beam elements is supposed to be enough to represent the curved ribs. Compared with the straight beam elements, the curved beam elements, adopted in this paper, are more efficient since they are capable of transferring loads through the combined action of bending and stretching.

For each curved beam element, there are two nodes and each node has six degrees of freedom. Fig. 3 shows the nodal displacements of one segment arch rib at nodes  $UL_i$  and  $UL_j$ . The nodal displacement vectors with respect to the local coordinate system are represented by:

$$\{\delta'_{ULi}\} = [u'_{ULi} \quad v'_{ULi} \quad w'_{ULi} \quad \theta'_{xULi} \quad \theta'_{yULi} \quad \theta'_{zULi}]^T \quad (2a)$$

$$\{\delta'_{ULj}\} = [u'_{ULj} \quad v'_{ULj} \quad w'_{ULj} \quad \theta'_{xULj} \quad \theta'_{yULj} \quad \theta'_{zULj}]^T \quad (2b)$$

where the local curvilinear coordinates  $x'$ - $y'$ - $z'$  are defined with the  $x'$ -axis along the neutral axis of the beam. The  $y'$ -axis is in the normal direction and the  $z'$ -axis is in the bi-normal direction.

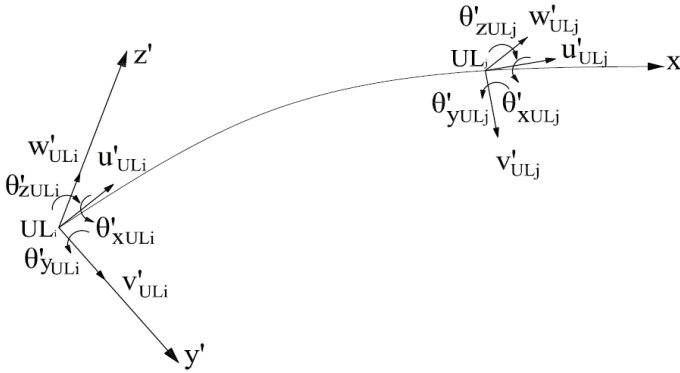


Figure 3: Nodal displacements of curved beam element

Based on the theory of curved beam [Yao (1989)], the displacements of an arbitrary point (denoted by  $k$  with coordinate  $x'$ ) of the curved beam element can be approximated as:

$$\begin{Bmatrix} u'_{ak} \\ v'_{ak} \\ \theta'_{xak} \end{Bmatrix} = [N_{a1}] \times [u'_{ULi} \quad v'_{ULi} \quad \theta'_{zULi} \quad u'_{ULj} \quad v'_{ULj} \quad \theta'_{zULj}]^T \quad (3a)$$

$$\{w'_{ak}\} = [N_{a2}] \times [w'_{ULi} \quad -\theta'_{yULi} \quad w'_{ULj} \quad -\theta'_{yULj}]^T \quad (3b)$$

$$\{\theta'_{yak}\} = [N_{a3}] \times [\theta'_{yULi} \quad \theta'_{yULj}]^T \quad (3c)$$

$$\{\theta'_{zak}\} = [N_{a4}] \times [\theta'_{zULi} \quad \theta'_{zULj}]^T \quad (3d)$$

with the shape functions  $[N_{a1}]$ ,  $[N_{a2}]$ ,  $[N_{a3}]$  and  $[N_{a4}]$  being shown as the following:

$$[N_{a1}] = \begin{bmatrix} 1 - \frac{x'}{l_a} & 0 & 0 \\ -\frac{x'}{r} + 2\frac{x'^2}{rl_a} - \frac{x'^3}{rl_a^2} & 1 - 3\frac{x'^2}{l_a} + 2\frac{x'^3}{l_a^2} & s - 2\frac{x'^2}{l_a} + \frac{x'^3}{l_a^2} \\ \frac{x'}{r} - 3\frac{x'^2}{rl_a^2} & -6\frac{x'}{l_a} + 6\frac{x'^2}{l_a^2} & 1 - 4\frac{x'}{l_a} + \frac{x'^3}{l_a^2} \\ & \frac{x'}{l_a} & 0 & 0 \\ & \frac{x'^2}{rl_a} - \frac{x'^3}{rl_a^2} & \frac{3x'^2}{l_a} - 2\frac{x'^3}{l_a^2} & -\frac{x'^2}{l_a} + \frac{x'^3}{l_a^2} \\ & 3\frac{x'}{rl_a} - 3\frac{x'^2}{r^2} & 6\frac{x'}{l_a^2} - 6\frac{x'^2}{l_a^3} & -2\frac{x'}{l_a} + 3\frac{x'^3}{l_a^3} \end{bmatrix} \quad (4a)$$

$$[N_{a2}] = \begin{bmatrix} 1 - 3\left(\frac{x'}{l_a}\right)^2 + 2\left(\frac{x'}{l_a}\right)^3 & x' - 2\frac{x'^2}{l_a} + \frac{x'^3}{l_a^2} & 3\left(\frac{x'}{l_a}\right)^2 - 2\left(\frac{x'}{l_a}\right)^3 & -\frac{x'^2}{l_a} + \frac{x'^3}{l_a^2} \end{bmatrix} \quad (4b)$$

$$[N_{a3}] = \begin{bmatrix} 1 - 6\frac{x'}{l_a^2} + 6\frac{x'^2}{l_a^3} & 1 - 4\frac{x'}{l_a} + \frac{3x'^2}{l_a^2} & 6\frac{x'}{l_a^2} - 6\frac{x'^2}{l_a^3} & -\frac{2x'}{l_a} + \frac{3x'^2}{l_a^2} \end{bmatrix} \quad (4c)$$

$$[N_{a4}] = \begin{bmatrix} 1 - \frac{x'}{l_a} & \frac{x'}{l_a} \end{bmatrix} \quad (4d)$$

in which the subscript  $a$  denotes the arch rib;  $u'_{ak}$ ,  $v'_{ak}$  and  $w'_{ak}$  denote displacements of arbitrary point along  $x'$ ,  $y'$  and  $z'$ -axis, respectively;  $\theta'_{xak}$ ,  $\theta'_{yak}$  and  $\theta'_{zak}$  denote rotations about  $x'$ ,  $y'$  and  $z'$ -axis, respectively;  $l_a$  is the length of the curved beam element;  $r$  is the curvature radius of the arch, which is assumed that the arch rib has a constant radius of curvature.

The displacements of the curved beam element presented above are in terms of the local coordinates, while the nodal displacements of the beam-arch segment are in the global co-ordinate system. Transforming displacements from the local coordinates to the global ones is required. The nodal displacement vectors of the curved beam element representing the arch rib with respect to global coordinate system are defined as:

$$\{\delta_{ULi}\} = [u_{ULi} \quad v_{ULi} \quad w_{ULi} \quad \theta_{xULi} \quad \theta_{yULi} \quad \theta_{zULi}]^T \quad (5a)$$

$$\{\delta_{ULj}\} = [u_{ULj} \quad v_{ULj} \quad w_{ULj} \quad \theta_{xULj} \quad \theta_{yULj} \quad \theta_{zULj}]^T \quad (5b)$$

Then the relationship between the nodal displacement vector with respect to local coordinate system and that with respect to global coordinate system is given by

$$\begin{Bmatrix} \delta'_{ULi} \\ \delta'_{ULj} \end{Bmatrix} = [\lambda] \begin{Bmatrix} \delta_{ULi} \\ \delta_{ULj} \end{Bmatrix} \quad (6)$$

where

$$[\lambda] = \begin{bmatrix} \lambda_1 & & & \\ & \lambda_1 & & \\ & & \lambda_2 & \\ & & & \lambda_2 \end{bmatrix}$$

$$\text{in which } [\lambda_1] = \begin{bmatrix} \cos \alpha_1 & \sin \alpha_1 & 0 \\ -\sin \alpha_1 & \cos \alpha_1 & 0 \\ 0 & 0 & 1 \end{bmatrix}; [\lambda_2] = \begin{bmatrix} \cos \alpha_2 & \sin \alpha_2 & 0 \\ -\sin \alpha_2 & \cos \alpha_2 & 0 \\ 0 & 0 & 1 \end{bmatrix}$$

where  $\alpha_1$  denotes the angle between two sets of axes at node  $UL_i$  and  $\alpha_2$  denotes the angle at node  $UL_j$ . The displacements of arbitrary point of the curved element in the global co-ordinates can be determined accordingly.

The axial strain  $\epsilon_{ak}$ , curvatures  $\kappa_{zak}$  and  $\kappa_{yak}$  about  $z'$  and  $y'$  axes, as well as torsional curvature  $\kappa_{xak}$  can be derived from:

$$\epsilon_{ak} = \frac{du'_{ak}}{dx'} - \frac{v'_{ak}}{r} \quad (7a)$$

$$\kappa_{zak} = \frac{d^2v'_{ak}}{dx'^2} + \frac{v'_{ak}}{r^2} \quad (7b)$$

$$\kappa_{yak} = \frac{d^2w'_{ak}}{dx'^2} - \frac{\theta'_{xak}}{r} \quad (7c)$$

$$\kappa_{xak} = \frac{d\theta'_{xak}}{dx'} + \frac{1}{r} \frac{dw'_{ak}}{dx'} \quad (7d)$$

For a curved arch rib beam element, the axial strain energy  $U_{a1}$ , flexural strain energies  $U_{a2}$  and  $U_{a3}$  about  $z'$  and  $y'$  axes, as well as torsional strain energy  $U_{a4}$  can be further calculated from

$$U_{a1} = \frac{1}{2} E_a A_a \int_0^{l_a} \epsilon_{ak}^2 dx' \quad (8a)$$

$$U_{a2} = \frac{1}{2} E_a I_{za} \int_0^{l_a} \kappa_{zak}^2 dx' \quad (8b)$$

$$U_{a3} = \frac{1}{2} E_a I_{ya} \int_0^{l_a} \kappa_{yak}^2 dx' \quad (8c)$$

$$U_{a4} = \frac{1}{2} G_a I_{da} \int_0^{l_a} \kappa_{xak}^2 dx' \quad (8d)$$

where  $E_a$  is Young's modulus of the arch rib;  $A_a$  is the sectional area;  $l_a$  is the length of the curved element;  $G_a$  is shear modulus of t of the arch rib;  $I_{ya}$  and  $I_{za}$  are the inertia moment about  $y'$  and  $z'$  axis;  $I_{da}$  is the polar inertia moment.

Therefore, the total elastic strain energy of the arch rib segment with nodes  $UL_i$  and  $UL_j$  are

$$U_a = U_{a1} + U_{a2} + U_{a3} + U_{a4} \quad (9)$$

Moreover, the potential energy of inertia force is defined as the negative value of work done by constant value of the inertia force:

$$V_a = m_a \int_0^{l_a} (u'_{ak} \ddot{u}'_{ak} + v'_{ak} \ddot{v}'_{ak} + w'_{ak} \ddot{w}'_{ak}) dx' \quad (10)$$

where  $m_a$  is the mass of arch rib's unit length.

#### 1.4 Consideration of suspenders

The elements used to simulate the suspenders in a beam-arch segment assembly are the truss element having three degrees-of-freedom per node as shown in Fig. 4. The nodal displacement vector of a suspender with nodes  $UL_i$  and  $LL_i$  in the local coordinate system is represented by:

$$\{\delta'_s\} = \begin{Bmatrix} u'_{ULi} & u'_{LLi} \\ v'_{ULi} & v'_{LLi} \\ w'_{ULi} & w'_{LLi} \end{Bmatrix} \quad (11)$$

The suspender displacements of an arbitrary point (denoted by  $k$ ) can be calculated from the shape functions and the nodal displacements:

$$\begin{Bmatrix} u'_{sk} \\ v'_{sk} \\ w'_{sk} \end{Bmatrix} = [IN_{s1} \quad IN_{s2}] \{\delta'_s\} \quad (12)$$

where the subscripts denotes the suspender and  $I$  is a three by three identity matrix. The shape functions with a linear interpolation are given as:

$$N_{s1} = 1 - y'/l_s; \quad N_{s2} = y'/l_s \quad (13)$$

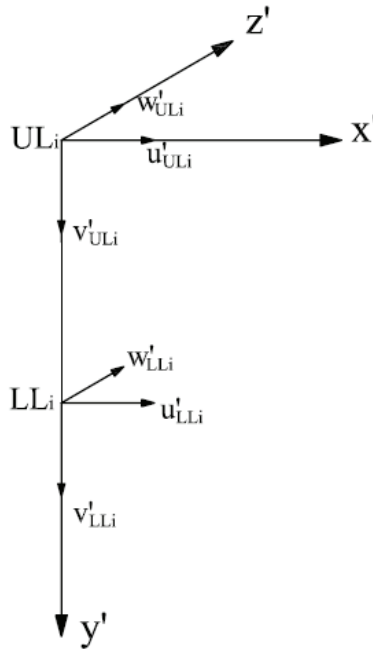


Figure 4: Nodal displacements of suspender element

in which  $y'$  is the coordinate along the axis of the suspender in the local co-ordinates and  $l_s$  is the length of the suspender.

The axial strain  $\epsilon_{sk}$  of a suspender element can be determined as:

$$\epsilon_{sk} = \frac{dv'_{sk}}{dy'} \tag{14}$$

The axial strain energy  $U_s$  of the suspender with nodes  $UL_i$  and  $LL_i$  can be calculated from:

$$U_s = \frac{1}{2}E_sA_s \int_0^{l_s} \epsilon_{sk}^2 dy' = \frac{1}{2}E_sA_s \int_0^{l_s} \left( \frac{dv'_{sk}}{dy'} \right)^2 dy' \tag{15}$$

where  $E_s$  is Young's modulus of the suspender and  $A_s$  is the area of its cross section. Similarly, the potential energy of the suspender is the work done by constant value of the inertia force:

$$V_s = m_s \int_0^{l_s} (u'_{sk}\ddot{u}'_{sk} + v'_{sk}\ddot{v}'_{sk} + w'_{sk}\ddot{w}'_{sk}) dy' \tag{16}$$

in which  $m_s$  is the mass of the suspender's unit length. The total energies for other three suspenders in a beam-arch segment assembly as shown in Fig. 1 can be determined in the same way.

### 1.5 Consideration of floor beams

The elements used to simulate the floor beams in a beam-arch segment assembly are the spatial beam element having six degrees-of-freedom per node as shown in Fig. 5. Taking the floor beam with nodes  $LL_i$  and  $LR_i$  in the local coordinate system as an example, the nodal displacement vector is represented by:

$$\{\delta'_f\} = \begin{Bmatrix} \delta'_{LLi} \\ \delta'_{LRi} \end{Bmatrix} \quad (17)$$

where

$$\{\delta'_{LLi}\} = \begin{Bmatrix} u'_{LLi} & \theta'_{xLLi} \\ v'_{LLi} & \theta'_{yLLi} \\ w'_{LLi} & \theta'_{zLLi} \end{Bmatrix}; \quad \{\delta'_{LRi}\} = \begin{Bmatrix} u'_{LRi} & \theta'_{xLRi} \\ v'_{LRi} & \theta'_{yLRi} \\ w'_{LRi} & \theta'_{zLRi} \end{Bmatrix} \quad (18)$$

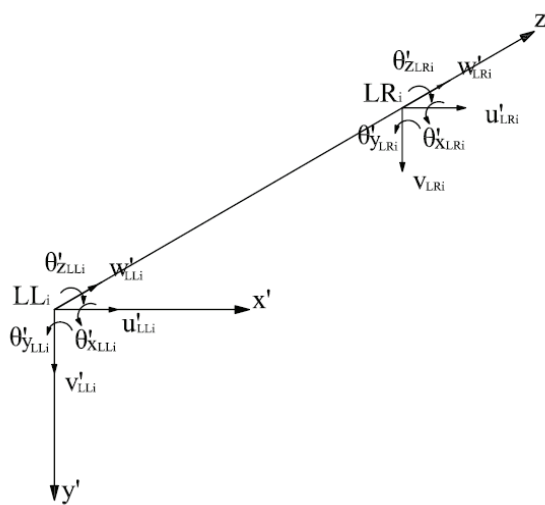


Figure 5: Nodal displacements of floor beam element

The displacements of an arbitrary point (denoted by  $k$ ) in the floor beam can be

calculated from the shape functions and the nodal displacements:

$$\begin{Bmatrix} u'_{fk} \\ v'_{fk} \\ w'_{fk} \\ \theta'_{x'fk} \\ \theta'_{y'fk} \\ \theta'_{z'fk} \end{Bmatrix} = \begin{bmatrix} N_{f1} \\ N_{f2} \\ N_{f3} \\ N_{f4} \\ N_{f5} \\ N_{f6} \end{bmatrix} \{\delta'_f\} \quad (19)$$

where the subscript  $f$  denotes the floor beam. The shape functions of the beam element are given as:

$$[N_{f1}] = \begin{bmatrix} 1 - \frac{3z'^2}{l_f^2} + \frac{2z'^3}{l_f^3} & 0 & 0 & 0 & -\left(z' - \frac{2z'^2}{l_f} + \frac{z'^3}{l_f^2}\right) & 0 & \frac{3z'^2}{l_f^2} - \frac{2z'^3}{l_f^3} \\ & & & & 0 & 0 & 0 - \left(-\frac{z'^2}{l_f} + \frac{z'^3}{l_f^2}\right) & 0 \end{bmatrix} \quad (20a)$$

$$[N_{f2}] = \begin{bmatrix} 0 & 1 - \frac{3z'^2}{l_f^2} + \frac{2z'^3}{l_f^3} & 0 & \left(z' - \frac{2z'^2}{l_f} + \frac{z'^3}{l_f^2}\right) & 0 & 0 & 0 & \frac{3z'^2}{l_f^2} - \frac{2z'^3}{l_f^3} \\ & & & & 0 & -\frac{z'^2}{l_f} + \frac{z'^3}{l_f^2} & 0 & 0 \end{bmatrix} \quad (20b)$$

$$[N_{f3}] = [0 \quad 0 \quad 1 - \frac{z'}{l_f} \quad 0 \quad 0 \quad 0 \quad 0 \quad 0 \quad \frac{z'}{l_f} \quad 0 \quad 0 \quad 0] \quad (20c)$$

$$[N_{f4}] = [0 \quad 0 \quad 0 \quad 1 - \frac{z'}{l_f} \quad 0 \quad 0 \quad 0 \quad 0 \quad 0 \quad 0 \quad \frac{z'}{l_f} \quad 0] \quad (20d)$$

$$[N_{f5}] = [0 \quad 0 \quad 0 \quad 0 \quad 1 - \frac{z'}{l_f} \quad 0 \quad 0 \quad 0 \quad 0 \quad 0 \quad \frac{z'}{l_f} \quad 0] \quad (20e)$$

$$[N_{f6}] = [0 \quad 0 \quad 0 \quad 0 \quad 0 \quad 1 - \frac{z'}{l_f} \quad 0 \quad 0 \quad 0 \quad 0 \quad 0 \quad \frac{z'}{l_f}] \quad (20f)$$

In which  $z'$  is the coordinate along the axis of the beam in the local co-ordinates and  $l_f$  is the length of the floor beam. The displacements with respect to the local coordinate system can be transformed to a global system following a similar pattern as the curved beam does.

Furthermore, the axial strain  $\epsilon_{fk}$ , the curvatures  $\kappa_{x'fk}$  and  $\kappa_{y'fk}$  about  $x'$  and  $y'$  axes, as well torsional curvature  $\kappa_{z'fk}$  can be calculated as follows:

$$\epsilon_{fk} = \frac{dw'_{fk}}{dz'} \quad (21a)$$

$$\kappa_{xfk} = \frac{d^2 v'_{fk}}{dz'^2} \quad (21b)$$

$$\kappa_{yfk} = \frac{d^2 u'_{fk}}{dz'^2} \quad (21c)$$

$$\kappa_{zfk} = \frac{d\theta'_{zfk}}{dz'} \quad (21d)$$

Thus, the corresponding strain energy can be obtained by

$$U_{f1} = \frac{1}{2} E_f A_f \int_0^{l_f} \varepsilon_{fk}^2 dz' \quad (22a)$$

$$U_{f2} = \frac{1}{2} E_f I_{fx} \int_0^{l_f} \kappa_{xfk}^2 dz' \quad (22b)$$

$$U_{f3} = \frac{1}{2} E_f I_{fy} \int_0^{l_f} \kappa_{yfk}^2 dz' \quad (22c)$$

$$U_{f4} = \frac{1}{2} G_f I_{fd} \int_0^{l_f} \kappa_{zfk}^2 dz' \quad (22d)$$

where  $E_f$  and  $G_f$  are respectively Young's and shear modulus of the floor beam.  $A_f$  is the sectional area.  $l_f$  is the length of the floor beam.  $I_{xf}$  and  $I_{yf}$  are the inertia moment about  $x'$  and  $y'$  axes;  $I_{df}$  is the polar moment of inertia.

The total elastic strain energies of the floor beam can thus be obtained:

$$U_f = U_{f1} + U_{f2} + U_{f3} + U_{f4} \quad (23)$$

The potential energy of the floor beam is the work done by constant value of the inertia force:

$$V_f = m_f \int_0^{l_f} (u'_{fk} \ddot{u}'_{fk} + v'_{fk} \ddot{v}'_{fk} + w'_{fk} \ddot{w}'_{fk}) dz' \quad (24)$$

where  $m_f$  is the mass of the floor beam's unit length. The elastic strain energies and potential energy for the other floor beams in the beam-arch segment assembly can be obtained in the same way.

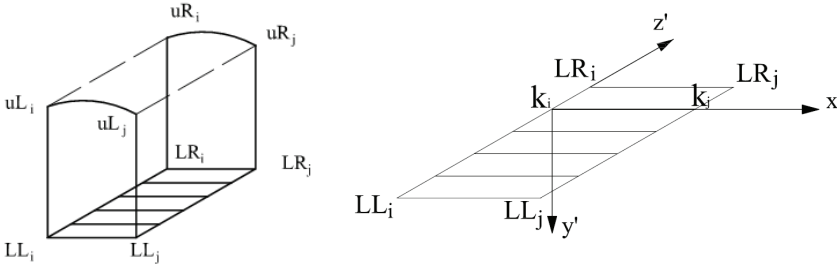


Figure 6: Bridge girder (stringer) segment

**1.6 Consideration of girders**

The bridge girders (tie bars) or stringers in a beam-arch segment assembly are also modeled by the spatial beam elements having six degrees-of-freedom per node as shown in Fig. 6. Once the nodal displacement vector of a girder segment in a local coordinate system are defined, similar to the floor beams, the displacements of a girder segment at an arbitrary point can be calculated by the shape functions of a standard beam element, and corresponding elastic strain energy  $U_{gk}$  as well as potential energy  $V_{gk}$  of the inertia force for the  $k$ th girder segment can be obtained. In addition, if there are the wind braces between two arches in a beam-arch segment assembly, the corresponding elastic strain energy and potential energy of the inertia force can be calculated in a similar way of floor beams.

**1.7 Total energies of a beam-arch segment assembly**

The total potential energy of elastic force and the potential energy of inertia force in a beam-arch segment assembly are the sum of their counterparts in each sub-element. It is worth noting that each suspender and floor beam is shared by two adjacent segments. What is meant by this is that a half of their energy contribution should be included in each beam-arch segment assembly. Consequently, the total potential energy of elastic force for the  $e$ th beam-arch segment assembly as shown in Fig. 2 can be directly formulated as follows:

$$U^e = U_a^e + \frac{U_s^e}{2} + \frac{U_f^e}{2} + U_g^e \tag{25}$$

where

$$U_a^e = U_a^{UL_i-UL_j} + U_a^{UR_i-UR_j} \tag{26a}$$

$$U_s^e = U_s^{UL_i-LL_i} + U_s^{UL_j-LL_j} + U_s^{UR_i-LR_i} + U_s^{UR_j-LR_j} \quad (26b)$$

$$U_f^e = U_f^{LL_i-LR_i} + U_f^{LL_j-LR_j} \quad (26c)$$

$$U_g^e = \sum_{k=1}^{N1} U_{gk} \quad (26d)$$

in which  $N1$  is the total number of stripes that the bridge deck can be divided into. Likewise, the total potential energy of inertia force can be also formulated as follows:

$$V^e = V_a^e + \frac{V_s^e}{2} + \frac{V_f^e}{2} + V_g^e \quad (27)$$

where

$$V_a^e = V_a^{UL_i-UL_j} + V_a^{UR_i-UR_j} \quad (28a)$$

$$V_s^e = V_s^{UL_i-LL_i} + V_s^{UL_j-LL_j} + V_s^{UR_i-LR_i} + V_s^{UR_j-LR_j} \quad (28b)$$

$$V_f^e = V_f^{LL_i-LR_i} + V_f^{LL_j-LR_j} \quad (28c)$$

$$V_g^e = \sum_{k=1}^{N1} V_{gk} \quad (28d)$$

## 2 Stiffness and mass matrices of a beam-arch segment assembly

To directly formulate the mass matrix and stiffness matrix of the beam-arch segment assembly, the principle of total potential energy with stationary value in elastic dynamics system and the “set-in-right-position” rule for formulating matrixes [Zeng and Guo (1999); Zeng (2000)] are used. With the aid of inertia forces (d’Alembert’s principle), the governing equations of motion in structural dynamics can be represented by the equations of dynamic equilibrium. It follows that the vibrating structure is in equilibrium under the action of a set of forces including the inertia force, elastic interactive force, damping force and external loads at any instant time. From the principle of virtual work, the system dynamic equilibrium equations can be formulated as

$$\delta \Pi = 0 \quad (29)$$

where  $\Pi$  is the total potential energy of dynamic system. It is worthwhile to note that the variational operation  $\delta$  should only be performed on the displacements or natural deformations of system, whereas all the forces are treated as invariants. As

an extension of the principle of stationary potential energy in statics to deal with the dynamic problems, the spatial vibration equations can be methodically and easily formulated by above principle.

To formulate the stiffness and mass matrices in finite element method, the dynamic equilibrium of system (Eq. (29)) can be rewritten in the following form if an elastic system has  $n$  degrees of freedom

$$\delta \Pi = \sum_{i=1}^n \frac{\partial \Pi}{\partial u_i} \delta u_i = 0 \quad (30)$$

Since  $\delta u_i$  is arbitrarily chosen and not equal to zero, thus, one has:

$$\delta u_1 \frac{\partial \Pi}{\partial u_1} = 0, \quad \delta u_2 \frac{\partial \Pi}{\partial u_2} = 0, \quad \dots, \quad \delta u_n \frac{\partial \Pi}{\partial u_n} = 0 \quad (31)$$

Eq. (31) represents the governing differential equations of motion for the discretized dynamic system. In general, each of them contains acceleration, velocity and displacement of system. By categorizing these structural variables, a matrix form can be written as

$$\{\delta u\}^T ([M]\{\ddot{u}\}) + [C]\{\dot{u}\} + [K]\{u\} - \{P\} = 0 \quad (32)$$

where  $\{\ddot{u}\}$ ,  $\{\dot{u}\}$  and  $\{u\}$  are the vectors of acceleration, velocity and displacement.  $[M]$ ,  $[C]$  and  $[K]$  are system matrices.  $\{P\}$  is the vector of external load.  $\{\delta u\}$  is a diagonal matrix as given below

$$\{\delta u\} = \text{diag} \begin{bmatrix} \delta u_1 & \cdots & 0 \\ \vdots & \ddots & \vdots \\ 0 & \cdots & \delta u_n \end{bmatrix}_{(n \times n)}$$

The reason to keep the item of  $\{\delta u\}^T$  in Eq. (32) is that it contains the important information to form the system matrices. From Eq. (31) and (32), it can be found that the symbol  $\delta u_i$  represents the  $i$ th row of  $[M]$ ,  $[C]$  and  $[K]$ , while  $\ddot{u}_j$ ,  $\dot{u}_j$  and  $u_j$  represents the  $j$ th column of  $[M]$ ,  $[C]$  and  $[K]$  respectively. Therefore, the coefficients in each terms of Eq. (32), which are multiplied by  $\delta u_i \ddot{u}_j$ ,  $\delta u_i \dot{u}_j$  and  $\delta u_i u_j$ , should be placed at the intersection position of the  $i$ th row and  $j$ th column of  $[M]$ ,  $[C]$  and  $[K]$  respectively. In addition, the coefficients only associated with  $\delta u_i$  should be placed at the  $i$ th row of  $\{P\}$ . This is the “set-in-right-position” rule for formulating system matrices. Since this rule is derived from  $\delta \Pi = 0$ , it allows to directly formulate the system matrices of the compound element or structure from

the total energy that is the sum of each simple sub-element or sub-system. This rule is helpful to form the system matrices of train-bridge vibration system [Zeng and Guo (1999)].

For the free vibration analysis without damping, the total potential energies of current beam-arch segment assembly include the elastic strain energy  $U^e$  and work  $V^e$  done by the inertia force upon the displacement measured from the reference point of potential energy. In such a case, Eq. (30) for a beam-arch segment assembly becomes

$$\delta \Pi = \sum_{i=1}^{N2} \frac{\partial U^e}{\partial u_i} \delta u_i + \sum_{i=1}^{N2} \frac{\partial V^e}{\partial u_i} \delta u_i = 0 \quad (33)$$

where  $u_i$  is the  $i$ th nodal displacement of the beam-arch segment assembly, while  $N2$  is the total number of nodal displacements of the beam-arch segment assembly. Thus the elemental stiffness matrix  $[k]^e$  that is associated with the first term in Eq. (33) and elemental mass matrix  $[m]^e$  that is associated with the second term in Eq. (33) can be formulated based on “set-in-right-position” rule.

Afterwards, the global mass matrix  $[[M]]$  and stiffness matrix  $[[K]]$  of the structure can be obtained by assembling all corresponding assembly matrixes:

$$[[M]] = \sum_{e=1}^{N3} [m]^e \quad (34a)$$

$$[K] = \sum_{e=1}^{N3} [k]^e \quad (34b)$$

where  $N3$  is the total number of beam-arch segment assembly.

Once the global mass and stiffness matrices are determined, the dynamic characteristic analysis is formulated by solving the eigenvalue problem:

$$([K] - \omega^2 [M]) \{\varphi\} = 0 \quad (35)$$

### 3 Case study

#### 3.1 Description of Jian concrete filled steel tubular arch bridge

To verify the applicability and efficiency of proposed beam-arch segment assembly procedure, a case of real arch bridge is studied. The bridge is the Jian Bridge located in Jian city, Jiangxi Province, China. It is a concrete filled steel tubular arch bridge. Fig. 7 shows a photograph of the completed bridge. The elevation and plan of the bridge are shown in Fig. 8. The bridge has a total length of

536 m, which consists of three concrete-filled steel tubular half-through arch spans (138m+188m+138m) and two symmetric side cantilevered half RC arch spans of 36 m.



Figure 7: Side view of the Jian Bridge

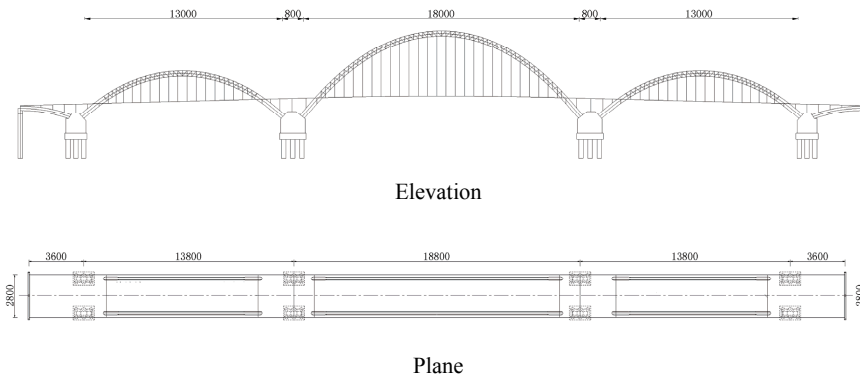


Figure 8: A general arrangement drawing of the bridge

The arch span has two parallel truss arch ribs, each of which has a triangular cross-section consisting of three steel tubes, with the dimensions of  $1,000 \times 16$  mm (the upper steel tube) and  $750 \times 12$  mm (the lower steel tubes). The steel tubes below the bridge deck are filled with high fluidity concrete. The depth of the arch rib

is 3,500 mm, and the width of the arch rib is 2,000 mm. The suspenders of the arch are the wire cables like those of suspension bridges. There are totally 120 suspenders spacing between 5 m to 6 m, which are vertically connected to the arch ribs and the floor beams of bridge deck. Each steel wire cable of the suspender has a diameter of 50 mm.

The deck load carrying system of the bridge consists of two main girders and floor beams. The girder is the I-beam arranged longitudinally with a different height depending on the position of the bridge. Two ends of the girder are connected by 16 pre-stressed steel strands acted as the tie bars to balance the horizontal forces arising from the arch. A reinforced concrete slab has a thickness of 600 mm.

### 3.2 Modeling with beam-arch segment assembly

In this paper, only the main span (188m) of the Jian bridge is considered in the analysis. The main span is divided into 31 beam-arch segment assemblies as shown in Fig. 9. Because the bridge is a half through arch bridge, the arch ribs and floor beams may be connected by either suspenders or columns, which leads to two kinds of beam-arch segment assemblies as shown in Fig. 10.

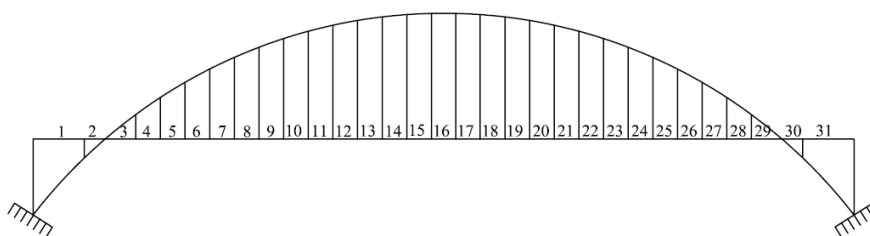


Figure 9: Segment discretization of Jian bridge main span

The curve of the arch rib is theoretically assumed by the catenaries, and its equation is defined as follows:

$$y = \frac{f}{m-1} \{ch[K(\frac{2x}{L})] - 1\} \quad (36)$$

where

$$K = \ln(m + \sqrt{m^2 - 1}) \quad (37)$$

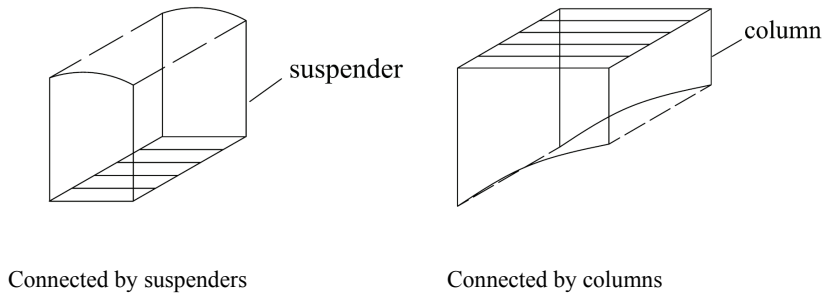


Figure 10: Two types of beam-arch segment

in which the length of the centre span is  $L=188\text{m}$ , the rise is  $f=54\text{m}$ , and the ratio of rise to span is  $m=0.3$ . Thus the geometric parameters of the arch rib such as the arch rib length  $l_a$ , curvature  $r$ , the angle  $\alpha$  between two sets of axes, suspender length  $l_s$  can be calculated from above equations and they are shown in Table 1. As the main span of the bridge is symmetric, the geometric parameters in Table 1 represent the half of the main span. The concrete filled steel tubular arch rib is considered as a composite material where the equivalent Young's modulus is used in the computation. The material parameters used in the analysis are summarized in Table 2.

The program of proposed beam-arch segment assembly procedure has been developed in the MATLAB environment. With the developed program, the free vibration (modal) analysis of the Jian bridge can be carried out and corresponding dynamic characteristics of the bridge such as natural frequencies and mode shapes can be obtained.

### 3.3 Modeling with ANSYS

To compare and validate the proposed beam-arch segment assembly procedure, a three-dimensional linear finite element model of the Jian Bridge is developed by ANSYS (1994), a commercial finite element analysis package. The arch ribs, girders, floor beams and other bracing members are modeled by the 3-D two node beam elements (BEAM4). All suspenders are modeled by the tension-only truss elements (LINK10). The deck concrete slab of the bridge is modeled by the shell elements (SHELL63). Solid elements (SOLID45) are used to model the platform of piers. The full 3-D view of the finite element model of the arch bridge is as shown in Fig. 11. With ANSYS, the free vibration (modal) analysis of the Jian

Table 1: Geometric parameters of the bridge

| Node | $l_a$ (m) | $r$ (m) | $\alpha$ (degree) | $l_s$ (m) |
|------|-----------|---------|-------------------|-----------|
| 1    | 10.50     | 254.15  | -52.93            | 16.37     |
| 2    | 10.72     | 223.96  | -50.56            | 8.11      |
| 3    | 8.02      | 199.44  | -47.82            | 0.00      |
| 4    | 8.37      | 179.54  | -45.51            | 5.83      |
| 5    | 8.01      | 161.25  | -42.84            | 11.67     |
| 6    | 7.67      | 145.26  | -34.00            | 16.97     |
| 7    | 7.36      | 131.40  | -36.97            | 21.74     |
| 8    | 7.08      | 119.47  | -33.76            | 26.00     |
| 9    | 6.84      | 109.32  | -30.37            | 29.77     |
| 10   | 6.62      | 100.81  | -26.79            | 33.04     |
| 11   | 6.43      | 93.82   | -23.03            | 35.83     |
| 12   | 6.28      | 88.24   | -19.10            | 38.14     |
| 13   | 6.16      | 83.99   | -15.03            | 39.98     |
| 14   | 6.07      | 81.01   | -10.83            | 41.36     |
| 15   | 6.03      | 79.23   | -6.53             | 42.28     |
| 16   | 6.00      | 78.65   | -2.18             | 42.74     |

Table 2: Physical parameters of the bridge

| Sub-structure              | Young's Modulus (MPa) | Poisson's ratio | Mass density (kg/m <sup>3</sup> ) |
|----------------------------|-----------------------|-----------------|-----------------------------------|
| Arch rib above bridge deck | $4.58 \times 10^4$    | 0.30            | 2800                              |
| Arch rib below bridge deck | $4.16 \times 10^4$    | 0.30            | 2550                              |
| Column                     | $5.66 \times 10^4$    | 0.30            | 2550                              |
| Suspender                  | $1.95 \times 10^5$    | 0.30            | 7850                              |
| Bridge deck                | $3.25 \times 10^4$    | 0.17            | 2500                              |

bridge can be carried out and corresponding dynamic characteristics of the bridge such as natural frequencies and mode shapes can be obtained.

### 3.4 Field ambient vibration tests of the bridge

The experimental modal analysis basically refers to the extraction of modal parameters (frequencies, damping ratios and mode shapes) from vibration measurements. These modal parameters can serve as a basis for finite element model updating verification and validation (V&V), structural damage detection, structural safety evaluation, and structural health monitoring. The controlled forced vibration testing by

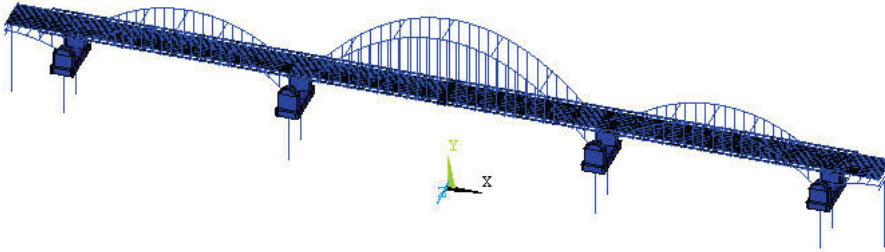


Figure 11: 3-D finite element model of the bridge

artificial means such as shakers or drop (releasing) weights is costly and difficult for intensively used bridges. In contrast, ambient vibration testing by using natural excitations such traffic, wind, pedestrian, and their combinations is a more feasible method for the bridges under operational conditions. Ambient vibration testing and modal parameter identification have been successfully applied to many bridges by authors and colleagues [Ren, Zhao and Harik (2004); Ren, Harik, Blandford, Lenett, Baseheart (2004); Ren, Zatar and Harik (2004); Ren, Peng and Lin (2005)]. The field dynamic testing on the Jian Bridge was carried out by using the method of ambient vibration. The equipments used to measure the acceleration-time responses consisted of 891-II accelerometers, cables and 32-channel data acquisition system. For the bridge deck, the accelerometers were directly placed on the surface of the bridge deck in the vertical direction as shown in Fig. 12. Measurement points were chosen on both upstream and downstream sides of the bridge at a location near the joint between the suspenders and deck. As a result, a total of 176 locations (88 points per side) were selected for acceleration measurements as shown in Fig. 13a. 18 test set-ups were used to cover the planned all measurement locations. Two reference (fixed) locations were selected for each set-up where one was in the center of the main span and another was near to the supporting of the main span. For the ambient vibration testing on the arch rib of the main span, 7 measurement locations as shown in Fig. 13b were instrumented with only one set-up.

#### Accelerometer placed on the deck surface Data Acquisition System

Once the measured time domain data are available from testing, the modal parameters (natural frequencies, damping ratios and mode shapes) can be identified from these data. The data processing and modal parameter identification were carried out by MACEC, a modal analysis toolbox for civil engineering construction [De Roeck and Peeters (1999)] where a rather simple peak-picking (PP) technique

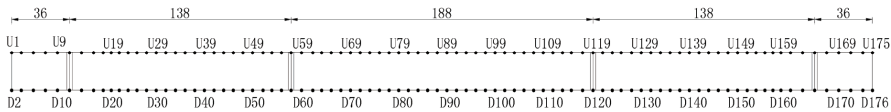


Accelerometer placed on the deck surface

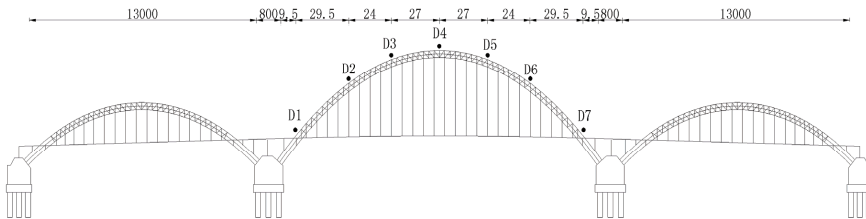


Data Acquisition System

Figure 12: Accelerometer and data acquisition system



(a)



(b)

Figure 13: Details of measurement locations

in frequency-domain and an advanced stochastic subspace identification (SSI) in time-domain are complementally used.

### 3.5 Results comparison and discussion

The natural frequencies of the main span and arch rib of the Jian bridge obtained from the proposed beam-arch segment assembly procedure, ANSYS and field ambient vibration testing are compared in Table 3 that presents the natural frequencies of first two vertical modes, the first two torsional modes of the bridge deck, and the

natural frequencies of first two vertical modes and transverse modes of the arch rib. Fig. 14 compares the mode shapes obtained from the beam-arch segment assembly procedure, ANSYS and field ambient vibration testing.

Table 3: Identified and calculated natural frequencies (Hz)

| Sub-structure | Modes          | Test  | Current method | Error (%) | ANSYS | Error (%) |
|---------------|----------------|-------|----------------|-----------|-------|-----------|
| Bridge deck   | 1st vertical   | 0.624 | 0.617          | 1.0       | 0.637 | 2.0       |
|               | 1st torsion    | 1.005 | 1.039          | 3.4       | 1.030 | 5.3       |
|               | 2nd vertical   | 1.063 | 1.092          | 2.7       | 1.079 | 1.5       |
|               | 2nd torsion    | 1.539 | 1.713          | 11.3      | 1.700 | 10.4      |
| Arch rib      | 1st vertical   | 0.624 | 0.617          | 1.0       | 0.637 | 2.0       |
|               | 2nd vertical   | 1.063 | 1.092          | 2.7       | 1.079 | 1.5       |
|               | 1st transverse | 0.303 | 0.221          | 27.0      | 0.224 | 26.0      |
|               | 2nd transverse | 0.594 | 0.583          | 1.9       | 0.512 | 13.8      |

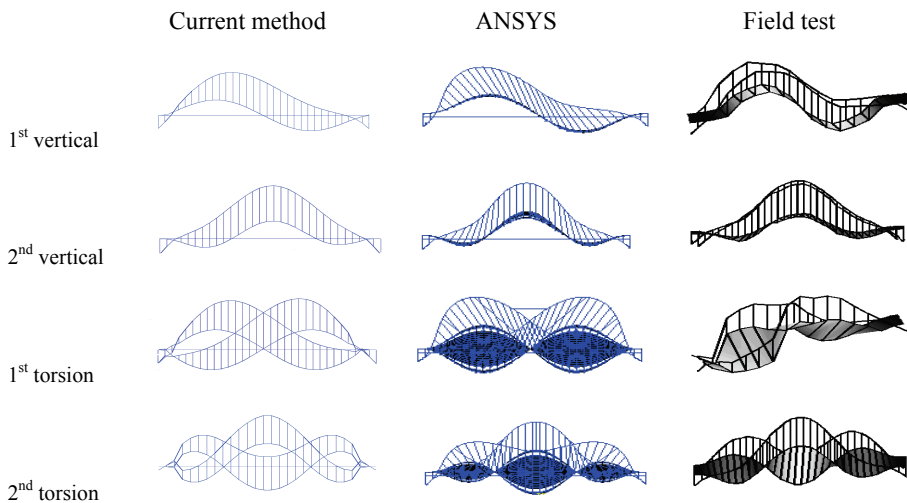


Figure 14: Comparison of mode shapes

It can be seen that both natural frequencies and mode shapes calculated from the proposed beam-arch segment assembly procedure agree well with those obtained

from the commercial finite element analysis package ANSYS and field ambient vibration testing. The proposed beam-arch segment assembly procedure is suitable and reliable for the dynamic analysis of arch bridges with less element numbers and enough accuracy.

It is demonstrated that the natural frequencies of the first and second vertical modes for the arch rib and the bridge deck are the same with the values of 0.623Hz and 1.063Hz. This means that the first two vertical vibrations of the arch rib and bridge deck occur simultaneously. However, the first transverse vibration of the arch rib of the Jian bridge shows a little bit low natural frequency of 0.303Hz.

#### 4 Concluding remarks

An efficient beam-arch segment assembly procedure for the dynamic analysis of arch bridges is presented in this paper. Such a beam-arch segment assembly is composed of different structural elements of arch bridges such as a curved-beam element for arch ribs, a truss element for suspenders and beam elements for floor beams and girders. Based on the principle of total potential energy with stationary value in elastic dynamics system, the stiffness matrix and mass matrix of such a compound assembly are derived in details. The corresponding MATLAB-based computer program is developed. The proposed beam-arch segment assembly procedure is then implemented to carry out the dynamics characteristics analysis of the Jian concrete filled steel tubular arch bridge in Jiangxi Province, China. Both natural frequencies and mode shapes of the Jian bridge calculated from the proposed beam-arch segment assembly procedure agree well with those obtained from the commercial finite element analysis package ANSYS and field dynamic testing under operational vibration conditions. It is demonstrated that the proposed beam-arch segment assembly procedure is suitable and reliable for the dynamic analysis of arch bridges with the advantages of less element numbers and enough accuracy. It is expected that this methodology can be an effective approach for the further dynamic response analysis of arch bridges under all kinds of dynamic loads such as earthquakes, winds and vehicles.

**Acknowledgement:** Financial supports from Research Fund for the Doctoral Program of Higher Education of China under grant number 20090162110051 and the Natural Science Foundation of China under grand number 51078357 are greatly acknowledged.

#### References

ANSYS (1994): *User's manual*, revision 5.3, Swanson Analysis System.

- Billington, D.P.** (1977): History and esthetics in concrete arch bridges. *Journal of the Structural Division, ASCE*, vol. 103, no. 11, pp. 2129-2143.
- Burden, A.R.** (1993): Japanese arch bridge design. *Proceedings of the Institution of Civil Engineers, Structures and Buildings*, vol. 99, no. 3, pp. 243-270.
- Calcada, R.; Cunha, A.; Delgado, R.** (2002): Dynamic analysis of metallic arch railway bridge. *Journal of Bridge Engineering, ASCE*, vol.7, no. 4, pp. 214-222.
- De Roeck, G.; Peeters, B.** (1999): *Manual of MACEC2.0—modal analysis on civil engineering constructions*, Department of Civil Engineering, Catholic University of Leuven, Belgium.
- Lee, B.K.; Wilson, J.F.** (1989): Free vibration of arches with variable curvature. *Journal of Sound and Vibration*, vol. 136, no. 1, pp. 75-89.
- Nazmy, A.S.** (1997): Stability and load-carrying of three-dimensional long-span steel arch bridges. *Computer & Structures*, vol. 65, no. 6, pp. 857-868.
- Nonaka, T.; Ali, A.** (2001): Dynamic response of half-through steel arch bridge using fiber model. *Journal of Bridge Engineering, ASCE*, vol. 6, no.6, pp. 482-488.
- Peng, D.M.; Fairfield, C.A.** (1999): Optimal design of arch bridges by integrating genetic algorithms and the mechanism method. *Engineering Structures*, vol. 21, no. 1, pp. 75-82.
- Qian, L.X.** (1987): New insight into an ancient stone arch bridge—the Zhao-Zhou Bridge of 1,400 years old. *International Journal of Mechanical Sciences*, vol. 29, no. 12, pp. 831-843.
- Raithel, A.; Franciosi, C.** (1984): Dynamic analysis of arches using Lagrangian approach. *Journal of Structural Engineering, ASCE*, vol. 110, no. 4, pp. 847-858.
- Ren, W.X.; Zong, Z.H.** (2004): Output-only modal parameter identification of civil engineering structures. *Structural Engineering and Mechanics*, vol. 17, no. 3-4, pp. 429-444.
- Ren, W.X.; Zhao, T.; Harik, I.E.** (2004): Experimental and analytical modal analysis of a steel arch bridge. *Journal of Structural Engineering, ASCE*, vol. 130, no. 7, pp. 1022-1031.
- Ren, W.X.; Harik, I.E.; Blandford, G.E.; Lenett, M.; Baseheart, T.M.** (2004): Roebling suspension bridge: II. ambient testing and live load response. *Journal of Bridge Engineering, ASCE*, vol. 9, no.2, pp. 119-126.
- Ren, W.X.; Zatar, W.; Harik, I.E.** (2004): Ambient vibration based seismic evaluation of highway bridges. *Engineering Structures*, vol. 26, no.5, pp. 629-638.
- Ren, W.X.; Peng, X.L.; Lin, Y.Q.** (2005): Experimental and analytical studies on dynamic characteristics of a large span cable-stayed bridge. *Engineering Struc-*

*tures*, vol. 27, no.4, pp. 535-548.

**Roeder, C.W.; Macrae, G.; Crocker, P.; Arima, K.; Wong, S.** (2000): Dynamic response and fatigue of steel tied-arch bridge. *Journal of Bridge Engineering, ASCE*, vol. 5, no. 1, pp. 14-21.

**Yao, L.S.** (1989): *Curve Beam*, China Communications Press, Beijing, China (in Chinese).

**Zeng, Q.Y.; Guo, X.R.** (1999): *Theory and application of vibration analysis of train-bridge time- dependent system*, China Railway Publishing House, Beijing (in Chinese).

**Zeng, Q.Y.** (2000): The principle of total potential energy with stationary value in elastic dynamic system. *Journal of Huazhong University of Science and Technology*, vol. 28, no. 1, pp. 1-3. (in Chinese)

**Zong, Z.H.; Jashi, B.; Ge, J.P.; Ren, W.X.** (2005): Dynamic analysis of a half-through concrete-filled tubular arch bridge. *Engineering Structures*, vol. 27, no. 1, pp. 3-15.